Journal of the American Society for Mass Spectrometry

pubs.acs.org/jasms Article

On the Origin of "Picket Fence" Peaks: Spectral Complexity, Mass Defect Uniformity, and Mass-to-Charge Ratio Alignment in Tandem Mass Spectra of Intact Proteins

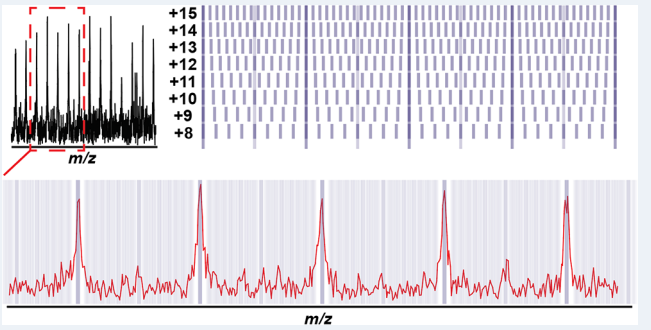
Published as part of Journal of the American Society for Mass Spectrometry special issue "Advances in Fourier Transform Mass Spectrometry".

Joshua D. Hinkle, Steven A. DeFiglia, Robert A. D'Ippolito, Christopher Mullen, Greg T. Blakney, Ping Yip, Romain Huguet, Kristina Håkansson, Jeffrey Shabanowitz, Donald F. Hunt, John E. P. Syka, and Lissa C. Anderson*

Cite This: https://doi.org/10.1021/jasms.6c00257 Read Online

ACCESS | Metrics & More | Article Recommendations | Supporting Information

ABSTRACT: Spectra from tandem mass spectrometry (MS/MS) of intact proteins are often highly complex, containing numerous closely spaced peaks arising from fragment ions with similar m/z values. This high level of spectral density continues to challenge even state-of-the-art high-resolution mass spectrometers, particularly as protein size increases. Here, we show that this complexity can produce a misleading spectral interference pattern when dissociating proteins whose fragment ions exhibit a sufficiently linear relationship between fragment mass and mass defect. In such cases, isotopic m/z peaks from multiple fragment ions constructively overlap to produce a series of predominantly ~1 m/z-spaced peaks, which we refer to as a "picket-fence" pattern. These peaks are easily misinterpreted as signals from much lower mass fragment ions ("peak at every mass" background) or distort expected isotopic peak envelopes. More fundamentally, these picket fence peaks can be understood as the collective manifestation of a high spectral density of signals arising from both sequence ions and the aggregate contribution of numerous individually low-abundance internal fragment ions. Recognizing and accounting for this often-observed phenomenon is essential for accurate fragment-ion assignment and interpretation of intact protein MS/MS spectra.



INTRODUCTION

Analysis of intact proteins by tandem mass spectrometry (MS/MS) is becoming an increasingly powerful approach for proteoform identification and sequencing.[1−4] Although traditional peptide-based MS/MS analysis following proteolytic digestion is both routine and robust, direct MS/MS analysis of intact proteins offers several attractive advantages. Characterization of proteoforms without digestion into smaller peptides allows determination of both intact mass and primary structure rather than requiring inference back to an intact proteoform based on only a peptide's limited sequence. Avoiding this so-called "protein inference problem" improves the ability to distinguish various—often closely related—proteoforms from one another.[5,6] Additionally, bypassing lengthy digestion steps has been shown to minimize the observation of artifact modifications such as deamidation or oxidation that often result from extensive sample handling.[7] Despite these advantages, obtaining primary structure information directly from large, intact proteins by MS/MS presents a substantial challenge, in part, due to the significantly increased spectral complexity.[8]

Compared to MS/MS spectra of peptides, intact protein MS/MS spectra contain far more unique fragment species (unique structures and molecular formulas). The number of possible fragment species increases sharply with protein size: the number of possible N- and C-terminal sequence fragment ion species increases linearly with the number of residues, while the number of possible internal fragment ion species (excluding single-residue fragments) scales quadratically. Each fragment can exhibit different isotopic compositions and be ionized to

Received: June 30, 2026
Revised: October 7, 2026
Accepted: October 9, 2026

ACS Publications © XXXX The Authors. Published by American Chemical Society

Downloaded from pubs.acs.org/jamsef/article-pdf/doi/10.1021/jasms.6c00257/6900474l/jasms.6c00257.pdf by FLORIDA STATE UNIV user on 02 November 2026

different charge states, each of which results in a unique mass-to-charge ratio (m/z).[8]

As a result, high resolution MS/MS spectra of intact proteins contain vastly more peaks than peptide spectra. Because charge is generally distributed relatively evenly along the backbone of a protonated, denatured protein, cleavage at most positions produces fragment ions that retain similar m/z values as the precursor ion.[9−11] For example, a fragment containing roughly half the backbone (and therefore about half the precursor mass) will often retain about half the precursor charges. This rough proportionality means that many of the first-generation product ions appear relatively close to the precursor m/z rather than being dispersed widely across the spectrum. The result is an exceptionally dense region of overlapping isotopic m/z peak distributions near the precursor m/z, making m/z and charge state assignment highly challenging. Overall, this fragmentation behavior causes fragment ion isotopic peak envelopes in MS/MS spectra of intact proteins to overlap far more frequently than is observed in peptide dissociation spectra—even when using high-resolution instrumentation.

Mann and others have noted that the possible intact masses of tryptic peptides are not uniformly distributed.[12,13] Although proteins exhibit a staggering degree of sequence diversity, the underlying chemical similarity among amino acids constrains the stoichiometry of their elemental composition. As a result, the fractional portions of peptide monoisotopic masses are not uniformly distributed. Within any 1 Da interval, peptide exact monoisotopic masses occupy a restricted range of possible values, making masses outside that range essentially impossible (or incredibly unlikely).[12,13]

This observation is equally applicable to fragment ions produced during dissociation of intact proteins. The fractional portions of the exact masses of protein fragment ions are similarly nonuniformly distributed, falling into restricted ranges of "allowed" fractional masses within any 1 Da interval, even for fragments of many kilodaltons. Thus, they have a higher tendency to occupy indistinguishably similar masses compared to a scenario where they were uniformly distributed. This mass restriction does not significantly complicate peptide MS/MS spectra due to the relatively small number of fragment ion species produced. However, in intact protein MS/MS spectra, signals from a much higher number of fragment ion species may be present in a relatively restricted portion of the m/z range such that numerous isotopic m/z peak envelopes overlap, frequently causing individual m/z peaks from multiple different fragment ion species to appear at the same m/z.

In this work, we demonstrate that, under these conditions, signals from highly charged fragment ion species can constructively reinforce at regular m/z intervals, producing a distinctive series of ∼1 m/z-spaced "picket fence" peaks. This series mimics the appearance of a series of m/z peaks from singly charged ion species, even though it originates from the superposition of multiple isotopic m/z peak envelopes. We also show that the likelihood of observing this phenomenon depends on the degree of proportionality between fragment mass defects and fragment nominal mass. These artifactual peak series significantly complicate spectral interpretation, distort isotopic envelopes beyond their expected intensity profile, and mislead automated algorithms for m/z peak assignment.

EXPERIMENTAL PROCEDURES

SILu Lite Antibody Preparation and Analysis

Samples of IdeS-digested SILu Lite monoclonal antibody (MilliporeSigma) were obtained from the Consortium for Top-Down Proteomics as part of their monoclonal antibody pilot study.[14] The antibody subunits were received frozen at a concentration of 1 μg/μL in a PBS buffer acidified with 0.05% trifluoroacetic acid. Prior to analysis, samples were reduced with 20 mM TCEP at 50 °C for 15 min, and ∼1 pmol was directly loaded onto a 10 cm PLRP-S (3 μm, 300 Å, Agilent Technologies) analytical column with the column heated to 42 °C. The proteins were separated online with a gradient of 30−42−100% Solvent B over 5−45−50 min (Solvent A: 0.3% formic acid in water; Solvent B: 0.3% formic acid in 72% acetonitrile, 18% isopropanol, and 9.7% water) and, after elution, were directly ionized into the inlet of the mass spectrometer at ∼60 nL/min.

Antibody subunits were analyzed with either a Thermo Scientific Orbitrap Fusion Tribrid or an in-house modified Orbitrap Elite.[15] Fragmentation was performed by high-energy collision dissociation (HCD) on the Orbitrap Fusion using stepped HCD collision energies of 21, 24, and 27% with an MS^2 automatic gain control (AGC) target of 1×10^6 precursor charges. Separately, the subunits were fragmented and charge-reduced by sequential electron transfer dissociation (ETD) and proton transfer charge reduction (PTCR) on the Orbitrap Elite.[9,16] For the ETD/PTCR experiments, 5 fragment ion fills of the C-trap were performed per transient signal acquisition with AGC targets of 1×10^5 precursor charges per fill and reagent targets of 7×10^4 and 3×10^5 for fluoranthene and perfluoromethyldecalin, respectively.[15] Additionally, a broadband-waveform auxiliary potential was applied between one pair of opposing rod electrodes of the linear ion trap during PTCR to perform parallel ion parking (PIP), arresting charge reduction once ions reached m/z 2500 to 3000 (the m/z range kinetically activated by the auxiliary potential), thereby concentrating signal in this region of the resulting spectra.[17−21]

To specifically evaluate whether the interference pattern could be dispersed by charge reduction, a separate experiment was performed on the SILu Lite Fd' subunit using the Orbitrap Elite. The 17^+ charge state precursor (m/z 1402) ions were first isolated in the linear ion trap and fragmented by (trap-type) resonant collision induced dissociation (CID) at 35% normalized collision energy. Fragment ions with m/z 1450 to 1500, corresponding to the most complex region of the MS^2 spectrum, were isolated and subjected to 15 ms of PTCR using sulfur hexafluoride radical anions. The PTCR reaction was performed with a precursor target of 1×10^5 and a reagent target of 3×10^5 for the PTCR reaction; the C-trap was filled with the products of 10 cycles of precursor accumulation and product ion generation before injection into the Orbitrap for m/z analysis.

Protein Standard Preparation and Analysis

Apomyoglobin samples were analyzed by direct infusion in 60% water, 40% acetonitrile, 0.1% acetic acid, or 50% water, 50% methanol, 0.1% formic acid at a concentration of 1 μM. Initial experiments were performed on an ultraviolet photo dissociation (UVPD)- and PTCR-enabled Orbitrap Fusion Lumos Tribrid mass spectrometer. The 20^+ charge state of apomyoglobin was isolated and subjected to 15 ms of UVPD using a 213 nm Crylas Nd:YAG ultraviolet laser. Fragment ions from m/z 650 to 680 were subsequently isolated and subjected to 0.75, 1.25, 2.5, and 5 ms PTCR reaction periods using nitrogenated fluoranthene (m/z 216). The intensities of picket fence peaks were monitored as a function of PTCR reaction duration.

Apomyoglobin was also analyzed on an Orbitrap Fusion Tribrid mass spectrometer. The 20^+ charge state of apomyoglobin (m/z 848) was fragmented by 1.5 ms of ETD and analyzed in the Orbitrap at 60,000, 120,000, 240,000, and 500,000 resolving power (at m/z 200). The intensities of picket fence peaks were monitored as a function of transient length to evaluate the influence of resolving power on the manifestation of picket fence m/z peak series in product ion spectra. ETD reactions were performed with a precursor target of 1×10^5 and a reagent target of 3×10^5.

Downloaded from pubs.acs.org/jamsef/article-pdf/doi/10.1021/jasms.6c00257/6900474l/jasms.6c00257.pdf by FLORIDA STATE UNIV user on 02 November 2026

https://doi.org/10.1021/jasms.6c00257
J. Am. Soc. Mass Spectrom. XXXX, XXX, XXX−XXX

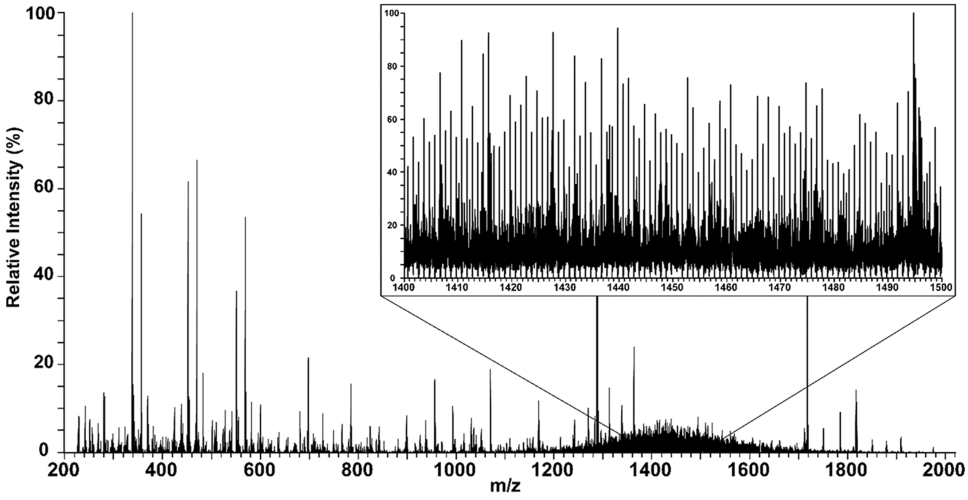


Figure 1. HCD MS/MS spectrum of the 18^+ charge state of the SILu Lite Fd' subunit. The inset shows an expanded view of the m/z 1400−1500 region, illustrating a ∼1 m/z-spaced picket fence interference pattern that extends across the densely populated region of the spectrum (∼m/z 1200−1700).

Carbonic anhydrase II was analyzed on a Thermo Scientific Orbitrap Eclipse Tribrid mass spectrometer modified with an infrared laser for concurrent photoactivation during activated-ion electron transfer dissociation (ai-ETD).[22] A selected precursor ion was isolated and fragmented by ai-ETD with a 1.5 ms ETD reaction time. Product ions were analyzed in the Orbitrap mass analyzer.

Bovine α-casein was desalted with 3 kDa molecular weight cutoff Amicon spin filters and prepared for direct infusion in 50% water, 50% methanol, 0.1% 1,5-diazobicyclo[4,3,0]non-5-ene[23] at a concentration of 5 μM. The sample was analyzed on a passively shielded 220 mm wide-bore 9.4 T Fourier-transform ion cyclotron resonance (FT-ICR) mass spectrometer equipped with a Tolmachev-style detection cell.[24−27] Electron detachment dissociation (EDD)[28−30] was performed on 29^- charge state precursor ions (m/z 813) of octuply phosphorylated α-casein. A −21 V potential was applied to the cathode for 300 ms, with the molybdenum grid biased to −17.6 V to regulate the number of electrons delivered to the cell.[31] After each irradiation event, a 100 ms electron cleanup delay occurred before excitation and detection of ions in the cell (3200 ms transient acquisitions, 8 megapoints). FT-ICR data were collected using Predator Acquisition v4.3.3 and processed with Predator Analysis v6.1.27[32] with various apodization functions as described in Figure S7. Different portions of the time-domain data were processed (i.e., time-frequency analysis) with the Predator Analysis software to evaluate the temporal dependence of picket fence m/z peaks.[33]

Mass Defect Calculations

Exact monoisotopic masses of predicted protein fragments were calculated from the molecular formulas of each fragment by summing the exact masses of the most abundant isotopes of the constituent elements (^{12}C, ^{1}H, ^{14}N, ^{16}O, ^{32}S, and ^{31}P).[34] The corresponding nominal masses for each fragment were calculated by summing the integer masses of these same isotopes, consistent with the IUPAC definition of nominal mass.[35,36] Note that these calculations differ from the floor-based definition sometimes used in peptide analyses, in which nominal mass is defined as the integer part of the total monoisotopic mass.[13] Subtracting the IUPAC-style nominal mass value from the monoisotopic mass yields the mass-defect quantity used in this study. Under the floor-based convention, mass-defect values are constrained to the interval between 0 and 1 Da and effectively reset at each nominal-mass boundary. In contrast, the present formulation preserves the cumulative contribution of atomic mass defects as fragment size increases, producing a continuous quantity that can exceed 1 Da and scales approximately linearly with fragment mass.[37] Importantly, the formulation used here preserves the monotonic dependence of fragment mass defect on fragment nominal mass, which is essential for modeling the proportionality trends underlying the interference phenomenon described here. The distinction between the two conventions is illustrated in Figure S1.

We define the quantity "fragment m/z defect" as the difference between the fragment ion's monoisotopic m/z value and the next lowest integer m/z value. This transformation is used solely for visualization to reveal geometric alignment and convergence in the m/z domain and does not redefine nominal mass or mass defect quantities, which are treated exclusively in the mass domain. Plotting these m/z defects for the most abundant isotopic m/z value arising from each fragment ion species highlights systematic alignments and convergence points that give rise to the observed picket-fence interference pattern.

RESULTS AND DISCUSSION

Observation of Unexplained ∼1 m/z Peak Series

In 2017, while analyzing monoclonal antibody standards for the second Consortium for Top-Down Proteomics pilot study,[14] students in the Hunt Laboratory at the University of Virginia observed a continuous ∼1 m/z-spaced peak series in MS/MS spectra of a reduced ∼25 kDa antibody subunit. In an Orbitrap HCD MS^2 spectrum of the SILu Lite heavy chain Fd′ subunit, the most complex region of the spectrum—spanning approximately m/z 1200−1700—exhibited a series of regularly spaced peaks at ∼1 m/z intervals (Figure 1). Peak spacings of ∼1 m/z would typically be attributed to singly charged ion species; however, this spectral region is expected to be dominated by signal from high-mass, highly charged fragment ion species. Comparable peak series were far less apparent, or absent, in MS/MS spectra of the associated light chain and Fc/2 subunits.

In parallel, scientists at Thermo Fisher Scientific's Life Sciences Mass Spectrometry (LSMS) facility in San Jose, California independently observed similar peak patterns with ∼1 m/z spacing in UVPD spectra of intact glycoproteins acquired in collaboration with the Pitteri Laboratory (Stanford University) on instruments under development at LSMS. To investigate the origin of these features, the UVA and LSMS teams jointly engaged collaborators at the National High Magnetic Field Laboratory (NHMFL, Tallahassee, FL) to acquire ultrahigh resolving power MS/MS spectra using a 21 T FT-ICR instrument, with the aim of resolving the overlapping m/z peaks hypothesized to give rise to the picket fence pattern. Notably, NHMFL scientists had independently observed similar

https://doi.org/10.1021/jasms.6c00257
J. Am. Soc. Mass Spectrom. XXXX, XXX, XXX−XXX

Downloaded from pubs.acs.org/jamsef/article-pdf/doi/10.1021/jasms.6c00257/6900474l/jasms.6c00257.pdf by FLORIDA STATE UNIV user on 02 November 2026

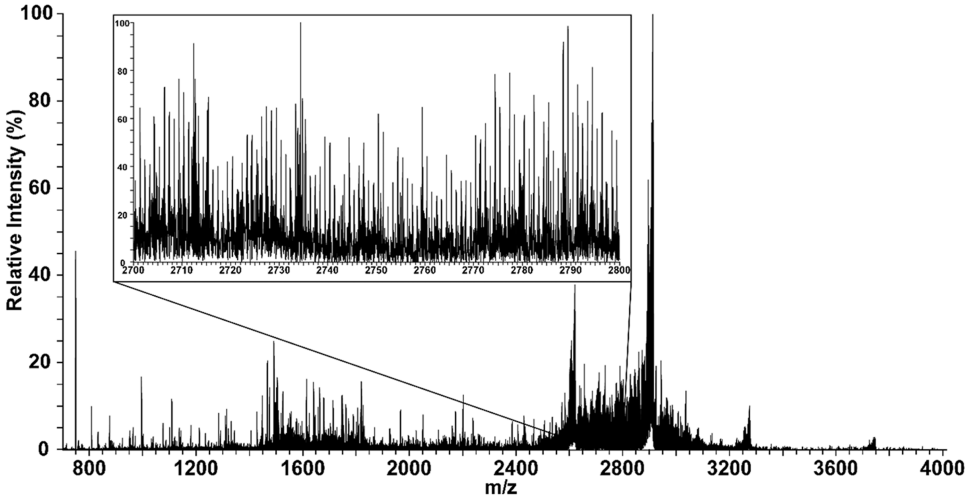


Figure 2. ETD/PTCR MS/MS spectrum of the 34^+ charge state of the SILu Lite Fd' subunit, acquired with PIP to arrest charge reduction once ions reached m/z 2300−2800. The inset highlights the ∼1 m/z-spaced interference pattern relocated to this region of the spectrum.

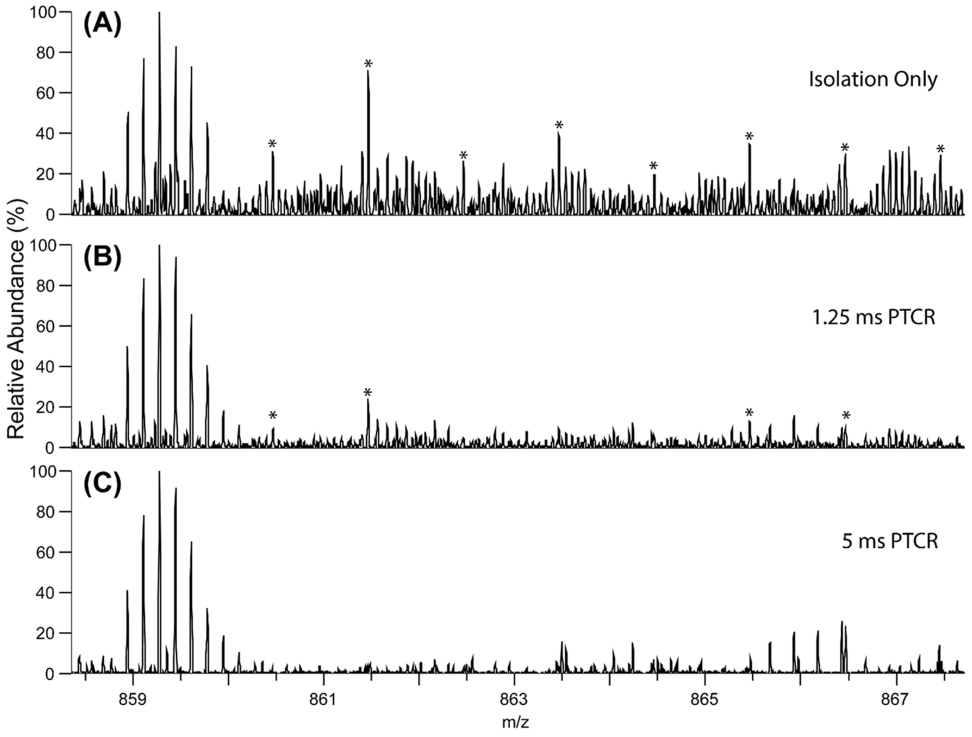


Figure 3. UVPD (15 ms) MS/MS spectrum of the 20^+ charge state of apomyoglobin following (A) 0, (B) 1.25, and (C) 5 ms of PTCR. Picket-fence peaks are marked with an asterisk and rapidly decrease in relative abundance with increasing PTCR reaction time.

∼1 m/z-spaced peak series in MS/MS spectra of intact SILu Lite heavy chain analyzed as part of the same antibody pilot study.[14]

These converging observations across multiple laboratories and instruments motivated a collaborative effort to determine the origin of this phenomenon and ultimately led to the development of the constructive interference model presented in this work.

Assessing the Origin of the ∼1 *m/z* Peak Series via Charge-State Analysis

To test whether the picket fence peak series observed in an ETD MS^2 spectrum of the SILu Lite Fd' subunit arose from truly singly charged ion species, charge manipulation experiments were performed. When these fragment ions were subjected to PTCR and PIP, the ∼1 m/z-spaced peak series from the original congested region of the MS^2 spectrum disappeared, and a new picket fence m/z peak series appeared in the ion parking window between m/z 2300 and 2800 (Figure 2) of the resulting MS^3 spectrum. This result demonstrates that the ∼1 m/z-spaced picket fence peak series originates from multiply charged ions rather than singly charged species, which would be neutralized and therefore not detected following a single PTCR reaction.

Additional experiments showed that, in the absence of PIP, the picket fence m/z peak pattern rapidly diminished upon charge reduction. In a UVPD MS/MS spectrum of the 20^+ charge state of apomyoglobin, another protein found to exhibit this behavior, a spectrally congested m/z region displayed a clear picket fence peak series prior to charge reduction (Figure 3A).

https://doi.org/10.1021/jasms.6c00257
J. Am. Soc. Mass Spectrom. XXXX, XXX, XXX−XXX

Downloaded from pubs.acs.org/jamsef/article-pdf/doi/10.1021/jasms.6c00257/6900741/jasms.6c00257.pdf by FLORIDA STATE UNIV user on 02 November 2026

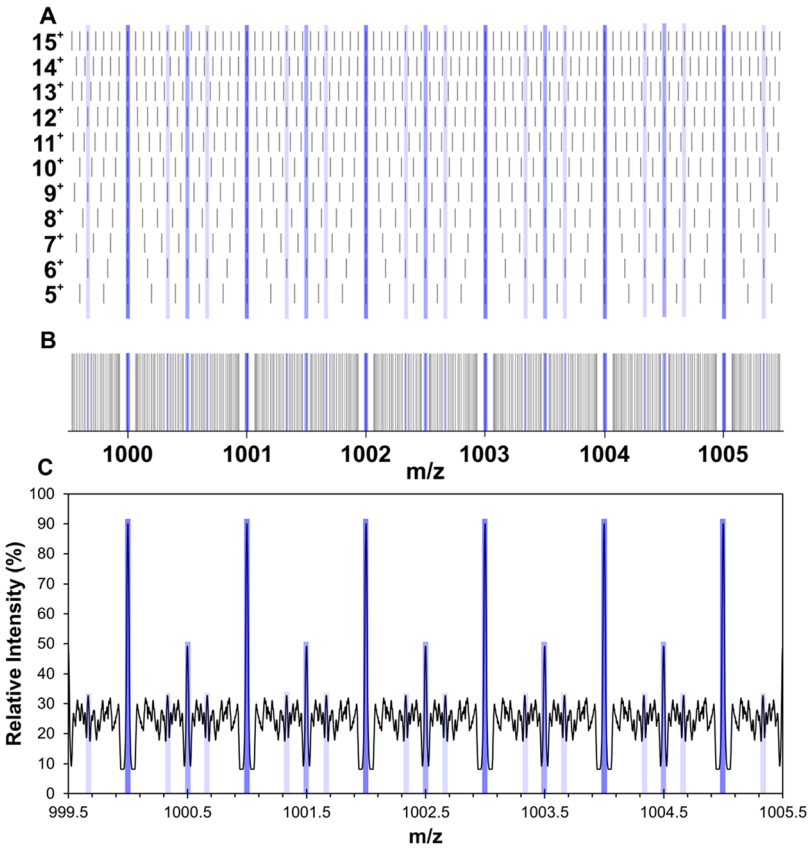


Figure 4. (A) Integer-mass peak combs for a hypothetical 10,000 Da fragment ion at charge states 5^+−15^+, shown individually as a function of m/z. For each charge state, comb positions appear at intervals of $1/|z|$ and are plotted within the m/z 999.5−1005.5 window. (B) Superposition of the corresponding combs from all charge states, with comb positions shown as vertical lines. Assuming zero mass defect, overlapping comb positions give rise to a dominant primary peak series with ∼1 m/z spacing. Secondary and tertiary series at 0.5 and 0.33 m/z, arise from coincidental alignment of subsets of charge states sharing common integer multiples of 2 and 3, respectively. (C) The same peak positions rendered as narrow half-cosine peaks for visual clarity, illustrating the resulting reinforced peak pattern.

However, after 1.5 and 5 ms of PTCR, these peaks were respectively reduced and eliminated in the corresponding MS^3 spectra (Figure 3B and C). Under these PTCR reaction conditions, ion−ion reaction rates scale approximately with the square of the precursor charge state, such that singly charged fragment ion populations would be expected to undergo complete charge neutralization on time scales significantly longer than 100 ms. The rapid depletion of these peaks within 5 ms therefore indicates that the contributing fragment ion species must carry substantially higher charge states, on the order of ∼7+ or greater.

These observations are consistent with an interference mechanism arising from the superposition of signals from multiple fragment ion species with similar m/z values in spectrally congested regions of the spectrum. As charge reduction proceeds, these fragment ions are redistributed to higher m/z values resulting in product ion spectra with fewer overlapping isotopic m/z peak envelopes from a multiplicity of fragment ion species and reducing the probability that they contribute signal at the same m/z value. Conversely, when PTCR is combined with PIP, charge-reduced fragment ions are concentrated into a relatively narrow m/z window and the picket-fence pattern re-emerges (Figure 2), consistent with the idea that the phenomenon is governed by overlap among multiply charged fragment-ion populations.

This behavior was reproduced in a similar experiment on a subregion of the SILu Lite Fd' product ion spectrum. In this experiment, the 17^+ charge state precursor was fragmented by ion trap-type resonant CID, producing a spectrally complex product ion m/z region containing a clear picket fence peak series in the MS^2 spectrum (Figure S2A). In a subsequent MS^3 experiment, the product ions from m/z 1450 to 1500 were isolated and subjected to PTCR (Figure S2B). Charge reduction significantly reduced the abundance of picket fence peaks within the isolation window and redistributed many highly charged fragment ion species to higher m/z values outside of the original isolation window. Many of these fragment ion species, which were not discernible as discrete isotopic m/z peak envelopes in the MS^2 spectrum, produced clearly resolved isotopic m/z peak envelopes after charge reduction.

Dependence of the Picket Fence Pattern on Fragment Mass-Defect Proportionality

To improve understanding of how fragment-ion m/z peaks can superpose to form an ∼1 m/z-spaced peak series, we begin with a simple illustrative model that considers the full set of all possible fragment masses up to that of the precursor. In this construction, fragment ions are represented by their integer neutral masses, and the proton mass is also treated as an exact integer. This integer-mass representation corresponds to describing each fragment species using the most abundant isotope of each constituent element, such that the nominal mass reflects the integer sum of the corresponding atomic mass numbers (i.e., the total number of protons and neutrons).

https://doi.org/10.1021/jasms.6c00257
J. Am. Soc. Mass Spectrom. XXXX, XXX, XXX−XXX

Downloaded from pubs.acs.org/jamsef/article-pdf/doi/10.1021/jasms.6c00257/6900474l/jasms.6c00257.pdf by FLORIDA STATE UNIV user on 02 November 2026

Under this assumption, the allowed fragment masses occupy a discrete integer sequence, and the m/z positions associated with fragments distributed across a given range of charge states form perfectly uniform "m/z peak combs" with spacing $1/z$ (Da per unit charge), such that for each charge state z, every zth peak falls at an integer m/z value (Figure 4A). To visualize how these combs relate to one another, their m/z periodicities can be examined within a narrow m/z window (e.g., m/z 999.5−1005.5), revealing a shared integer-based comb (Figure 4B). When these combs are overlaid, many peak positions coincide at regular m/z intervals, producing a prominent 1 m/z pattern of constructive reinforcement. Weaker secondary and tertiary reinforcement patterns are also observed as fractional spacings (e.g., 1/2 and 1/3 m/z), arising from constructive overlap among periodic m/z peak series corresponding to charge states that are integer multiples of 2 and 3.

Figure 4A shows the individual charge-state m/z peak combs, with each comb plotted separately as a vertical line to illustrate the charge-dependent spacing. Figure 4B shows these same combs overlaid within a limited m/z window, revealing the shared integer-based m/z grid and the resulting coincidence of peak positions. In Figure 4C, these same superposed peak-comb positions are rendered as small half-cosine peaks for visual clarity. In this representation, the underlying "grid" corresponds to the set of theoretical peak-comb positions, and the half-cosine shapes are used solely to render those positions in a more visually intuitive peak-like form. Although simplified, this construction establishes both a mathematical and visual basis for understanding the interference phenomenon that produces picket fence m/z peak series.

Of course, real protein fragments do not have integer mass values, nor do they correspond to single mass values. The masses of the most abundant isotopes of hydrogen, nitrogen, oxygen, and sulfur all differ slightly from their nominal integer values, and the exact monoisotopic mass of a fragment depends on its elemental composition. To evaluate how mass defects influence the appearance of reinforced m/z peaks, we consider the monoisotopic neutral mass, M_i, of fragment i, where the index i labels a specific fragment with a defined elemental composition. This mass can be expressed as

$$M_i = N_i + D_i \tag{1}$$

where N_i is the nominal mass (Da), obtained by summing the integer masses of the most abundant isotopes of each constituent element, and D_i is the corresponding monoisotopic mass defect (Da).

In this formulation, the numerical value of N_i serves as an integer mass that places each fragment on an idealized nominal-mass grid with 1 Da spacing. In this limited sense, N_i plays a role analogous to the atomic mass number—that is, a "molecularized" mass number reflecting the total nucleon count under the nominal-mass convention. Because proteins are composed of a limited and chemically similar set of amino acids, their fragments share broadly similar elemental compositions. Consequently, the monoisotopic mass defects of protein fragments exhibit an approximately proportional relationship with nominal masses, consistent with the principles underlying the averagine model.[38]

Here, we approximate this proportionality for any sequence fragment i using

$$D_i \approx k_{\text{fit}} N_i \tag{2}$$

where k_{fit} is a sequence-specific proportionality constant. We obtain k_{fit} by performing a least-squares fit of all calculated mass-defect values, D_i, against the corresponding nominal masses, N_i, for all expected terminal (N- and C-terminus-containing) sequence fragments generated from an *in silico* dissociation of the protein sequence. In this formulation, D_i is not constrained to values below 1 Da and can exceed 1 Da as fragment size increases. The fitted slope k_{fit} summarizes the overall mass-defect scaling behavior of the sequence and defines the monoisotopic mass-defect trendline used throughout the remainder of the analysis. For the results presented here, *c*- and *z*•-type terminal sequence fragments were considered as an illustrative example, although the observed mass-defect scaling behavior is not specific to these fragment-ion series; large internal fragments and alternative backbone cleavages (e.g., *b*- and *y*-type ions) exhibit the same behavior because the underlying proportionality arises from fragment elemental composition rather than fragmentation mechanism.

Figure 5 illustrates mass-defect proportionality for three representative proteins: apomyoglobin (∼17 kDa) and the SILu Lite Fd' subunit (∼25 kDa), both of which exhibit prominent picket-fence patterns in their MS/MS spectra, and carbonic anhydrase II (∼29 kDa), which does not exhibit the pronounced, extended picket-fence peak series observed for apomyoglobin and the SILu Lite Fd′ subunit. Shown are plots of monoisotopic mass defect versus nominal mass for *c*- and *z*•-type terminal sequence fragments from each protein. Each protein's sequence yields a slightly different k_{fit} value, reflecting differences in amino-acid composition and the corresponding elemental stoichiometry. For apomyoglobin and the SILu Lite Fd' subunit, fragment masses fall tightly along their fitted mass-defect trendlines, indicating strong proportional scaling with nominal mass. In contrast, fragments of carbonic anhydrase II scatter much more broadly around the fitted line, indicating poorer mass-defect proportionality. Notably, this broader dispersion reflects larger residuals about the mass-defect trendline, consistent with the weaker reinforcement behavior observed for carbonic anhydrase II.

For individual sequence fragments, the degree of deviation from this proportional trend can be modeled using a corresponding residual term, ε_i, such that the exact monoisotopic mass defect for fragment i can be written as

$$D_i = k_{\text{fit}} N_i + \varepsilon_i \tag{3}$$

The residual ε_i quantifies the deviation of each fragment's monoisotopic mass defect from the fitted mass-defect trendline (eq 2), reflecting fragment-specific variation in elemental stoichiometry not captured by the sequence-averaged proportionality described by k_{fit}. Fragments with compositions close to the average of all sequence fragments exhibit small residuals, whereas fragments enriched in elements with relatively higher or lower mass defects per unit nominal mass exhibit correspondingly larger positive or negative deviations from the fitted trendline. For example, acidic amino acid residues are enriched in oxygen, which contributes a lower mass defect per nominal mass, leading to lower mass-defect values for fragments enriched in these residues, whereas aliphatic residues are enriched in hydrogen, which contributes a higher mass defect per nominal mass and therefore leads to higher mass-defect values on the same basis.

While the approximately linear relationship between nominal mass and mass defect is consistent with the principles underlying the averagine model and is expected for protein fragments in general, the interference phenomenon described here is governed by the sequence-dependent residuals about that

Downloaded from pubs.acs.org/jamsef/article-pdf/doi/10.1021/jasms.6c00257/6900474l/jasms.6c00257.pdf by FLORIDA STATE UNIV user on 02 November 2026

https://doi.org/10.1021/jasms.6c00257
J. Am. Soc. Mass Spectrom. XXXX, XXX, XXX−XXX

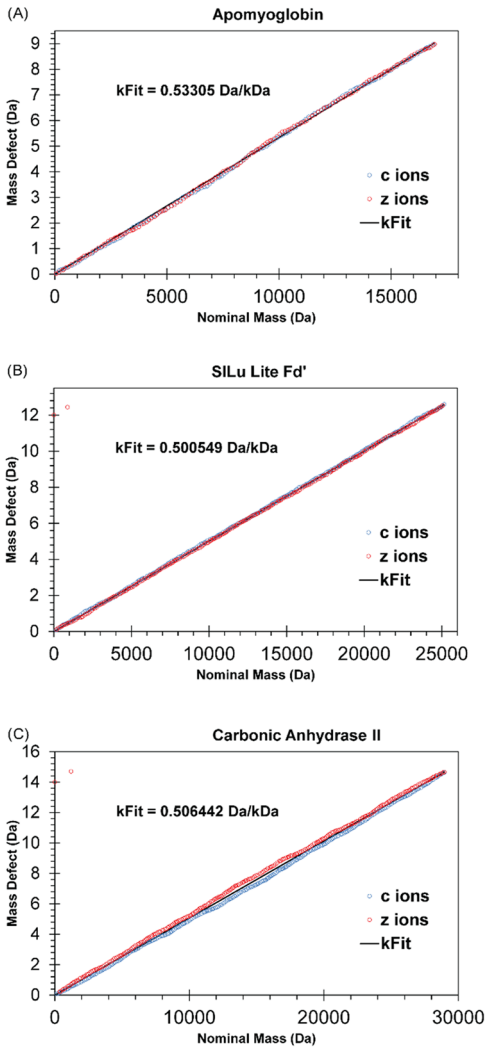


Figure 5. Plots of monoisotopic mass defect versus nominal mass for *c*-type (blue) and *z*•-type (red) fragment ions derived from (A) apomyoglobin, (B) the SILu Lite Fd′ subunit, and (C) carbonic anhydrase II. Apomyoglobin and the SILu Lite Fd′ subunit show tight linear trends, while carbonic anhydrase II exhibits broader scattering. These differences illustrate how the degree of mass-defect proportionality varies between protein sequences and underpins whether fragment ions are likely to reinforce at common m/z positions in complex MS/MS spectra.

trend. These residuals arise because amino acid composition is not evenly distributed along a protein sequence, causing individual fragment masses to deviate from the sequence-averaged mass-defect relationship. Consequently, two proteins may exhibit similar average mass-defect scaling while displaying markedly different residual distributions and, therefore, different propensities to generate reinforced m/z peak series. Averagine captures the average slope of the mass-defect relationship but does not predict the sequence-dependent residual structure that ultimately governs fragment-ion alignment and reinforcement in the m/z domain. Figure S3 shows these residuals plotted as a function of fragment nominal mass for each of the three proteins examined. These patterns reveal a clear correlation between the magnitude of these residuals and the likelihood that a protein's fragment-ion spectrum exhibits a picket-fence peak series. Residuals for carbonic anhydrase II (Figure S3A) are comparatively large, consistent with the absence of the pronounced, extended picket-fence peak series (Figure S4). Conversely, apomyoglobin and the SILu Lite Fd' subunit exhibit much smaller residuals (Figure S3B and C), consistent with their propensity to produce prominent, extended picket-fence peak series.

Substituting the fitted mass-defect relationship (eq 3) into the definition of monoisotopic mass (eq 1) expresses the exact monoisotopic neutral mass, M_i, of fragment i in fitted form as

$$M_i = N_i + k_{\text{fit}}N_i + \varepsilon_i = (1 + k_{\text{fit}})N_i + \varepsilon_i \tag{4}$$

Assuming ionization via protonation, the corresponding m/z for fragment ion i with charge state z (signed) is given by

$$[m/z]_i = \frac{(1 + k_{\text{fit}})N_i + \varepsilon_i + z[m/z]_{\text{Proton}}}{|z|} = \frac{(1 + k_{\text{fit}})}{|z|}N_i + \frac{\varepsilon_i}{|z|} + \frac{z}{|z|}[m/z]_{\text{Proton}} \tag{5}$$

where the $[m/z]_{\text{Proton}}$, (~1.00728 Da per elementary charge), is the contribution of the proton charge carriers to the product ion's m/z.

Inspection of this expression reveals that the contribution of the residual term, ε_i, to a particular fragment ion's exact monoisotopic m/z becomes smaller as the charge state increases (in inverse proportion to the magnitude of the charge state, $|z|$). Thus, for sufficiently small residuals, the contribution of ε_i to the m/z may become negligible for large fragment ions having relatively high charge states.

Under these conditions, the exact monoisotopic m/z values of fragment ions having a common charge state, z, will always be close to a series of evenly spaced "comb" m/z values defined by the expression

$$[m/z]_{\text{comb}} \approx \frac{(1 + k_{\text{fit}})}{|z|}N + \frac{z}{|z|}[m/z]_{\text{Proton}} \tag{6}$$

For each charge state, there is a one-to-one relationship between each (integer-valued) nominal mass and the corresponding comb m/z position, with spacing of the m/z peak centers of $(1 + k_{\text{fit}})/|z|$ Da/elementary charge. In the absence of mass defect ($k_{\text{fit}} = 0$), this expression reduces to the comb of m/z peaks described in the initial simplified model, with m/z spacing of $1/|z|$ Da/elementary charge but which is shifted by the proton m/z term, with a positive sign for protonated fragment ions and a negative sign for deprotonated fragment ions. Collectively, the m/z combs corresponding to all charge states will align at intervals of $(1 + k_{\text{fit}})$ Da/elementary charge. Combs associated with charge states that are integer multiples of 2 and 3 will also align at fractional intervals of $(1 + k_{\text{fit}})/2$ and $(1 + k_{\text{fit}})/3$ Da/elementary charge, respectively.

The extent to which the exact monoisotopic m/z of any particular fragment species (denoted by index i) aligns with a given comb position depends on the residual term $\varepsilon_i/|z|$. Fragments with smaller residuals therefore exhibit m/z values that lie closer to the corresponding comb positions. Accordingly, proteins whose fragment monoisotopic masses collectively have small residual terms produce fragment-ions with m/z values that more closely follow the comb structure. The present model does not predict that all proteins should exhibit equally strong picket-fence behavior. The intensity and extent of reinforcement are expected to vary continuously according to both spectral congestion and the degree of mass-defect proportionality. Consequently, proteins may exhibit reinforcement behavior of

Downloaded from pubs.acs.org/jamsef/article-pdf/doi/10.1021/jasms.6c00257/6900474l/jasms.6c00257.pdf by FLORIDA STATE UNIV user on 02 November 2026

https://doi.org/10.1021/jasms.6c00257
J. Am. Soc. Mass Spectrom. XXXX, XXX, XXX−XXX

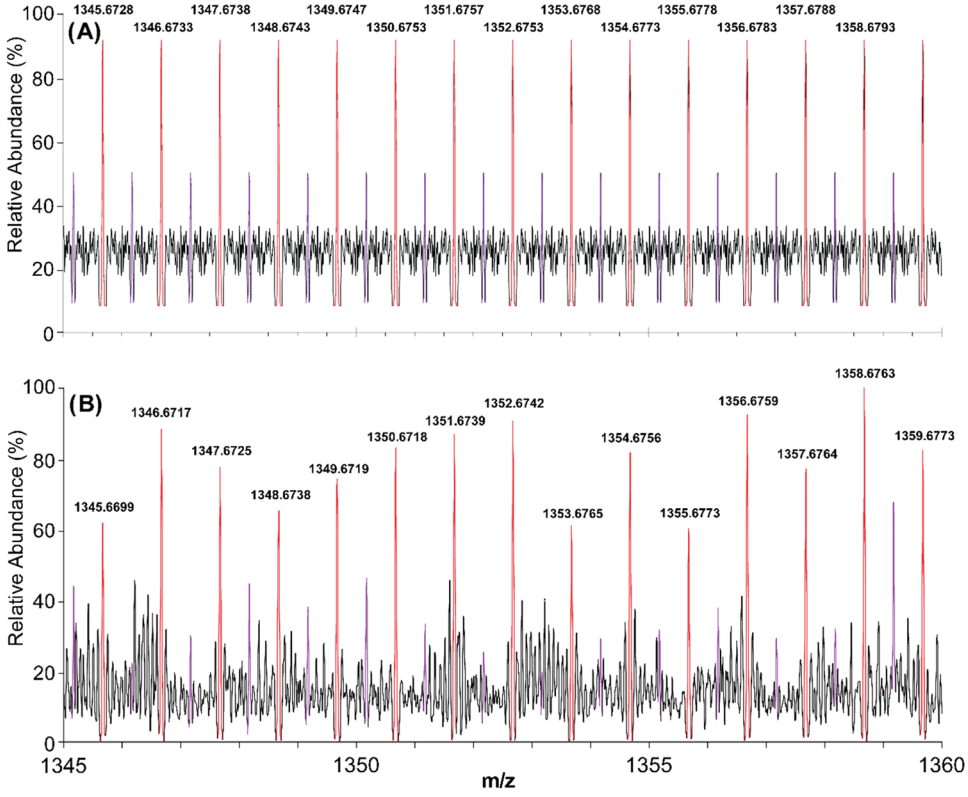


Figure 6. (A) Theoretical superposition of m/z peak combs for charge states 5^+ to 14^+ for the SILu Lite Fd' subunit, with comb spacing scaled by $(1 + k_{fit})/z$. (B) corresponding experimental HCD MS/MS spectrum of the SILu Lite Fd' subunit. In both panels, the primary (~1 m/z) and secondary (~0.5 m/z) reinforced peak series are highlighted (red and purple, respectively) to facilitate comparison between the modeled and experimental picket fence patterns.

varying intensity and extent depending on the distribution of fragment-ion residual terms and the complexity of the fragment-ion population. Spectral congestion is therefore necessary but not sufficient for the appearance of prominent, extended picket-fence peak series; strong mass-defect proportionality is also required. Accordingly, the three proteins examined here should be viewed as examples spanning a range of reinforcement behavior rather than as an exhaustive survey of protein sequence space.

Incorporating the corresponding k_{fit} value into the peak-comb model adjusts the spacing of the simulated monisotopic mass combs for a given protein sequence. Figure 6A illustrates this refinement for the SILu Lite Fd' subunit: the period of the half-cosine peak combs is adjusted such that the spacing of the m/z peak centers scales as $(1 + k_{fit})/|z|$. Note that this refinement affects only the spacing of the modeled combs; it does not depend on the exact monoisotopic masses M_i of individual fragments. With this adjustment, the model closely reproduces the appearance of the most congested regions of the SILu Lite Fd' HCD MS^2 spectrum (Figure 6B). The experimental data exhibit not only the primary ~1 m/z-spaced peak series, but also the secondary series spaced by ~1/2 m/z as predicted by the model. Strikingly, the predicted m/z values agree closely with the experiment: in the m/z 1345−1360 region, the root-mean-squared difference between the predicted and observed peak positions is 0.0021 m/z (1.58 ppm), well within the expected m/z assignment accuracy of the instrument.

While the peak-comb model captures the spacing of the reinforced m/z peaks arising from monoisotopic fragment masses, intact protein fragments appear in real spectra as full isotopic distributions rather than single mass values. In principle, isotopic variation could disrupt the reinforcement predicted by the model. In practice, however, the positions of isotopic peaks in the m/z domain are strongly constrained by two factors. First, isotopic substitutions introduce only small additional neutral-mass offsets relative to the nominal-mass comb for large protein fragments, resulting in deviations on the order of a few tens of mDa at most. Second, because intact protein fragments carry substantial charge, these neutral-mass offsets are divided by the charge state z in the m/z domain. As a result, the m/z spacing among isotopic peak centroids is compressed to a degree that makes these differences small relative to typical experimental peak widths, allowing the isotopic peaks of a fragment to follow essentially the same mass-defect trendline as the corresponding monoisotopic mass. This behavior is illustrated in Figure S5, which shows that even when isotopic fine structure becomes resolved at very high simulated resolving powers, isotopologue populations remain confined to a relatively narrow mass range within the broader isotopic envelope.

Under these conditions, isotopic peak centroids from different fragment ions can still align at predictable m/z positions and reinforce one another, even though they do not have identical neutral masses. This behavior is evident in Figure S6, which shows that, for proteins that exhibit strong picket-fence patterns, the centroids of the most abundant isotopic peaks from each fragment ion converge tightly within a narrow band in m/z-defect space, consistent with the underlying mass-defect proportionality defined by the k_{fit}. In contrast, proteins with poor mass-defect proportionality, such as carbonic anhydrase II, show much broader dispersion of isotopic peak centroids and do

Downloaded from pubs.acs.org/jamsef/article-pdf/doi/10.1021/jasms.6c00257/6900474l/jasms.6c00257.pdf by FLORIDA STATE UNIV user on 02 November 2026

https://doi.org/10.1021/jasms.6c00257
J. Am. Soc. Mass Spectrom. XXXX, XXX, XXX−XXX

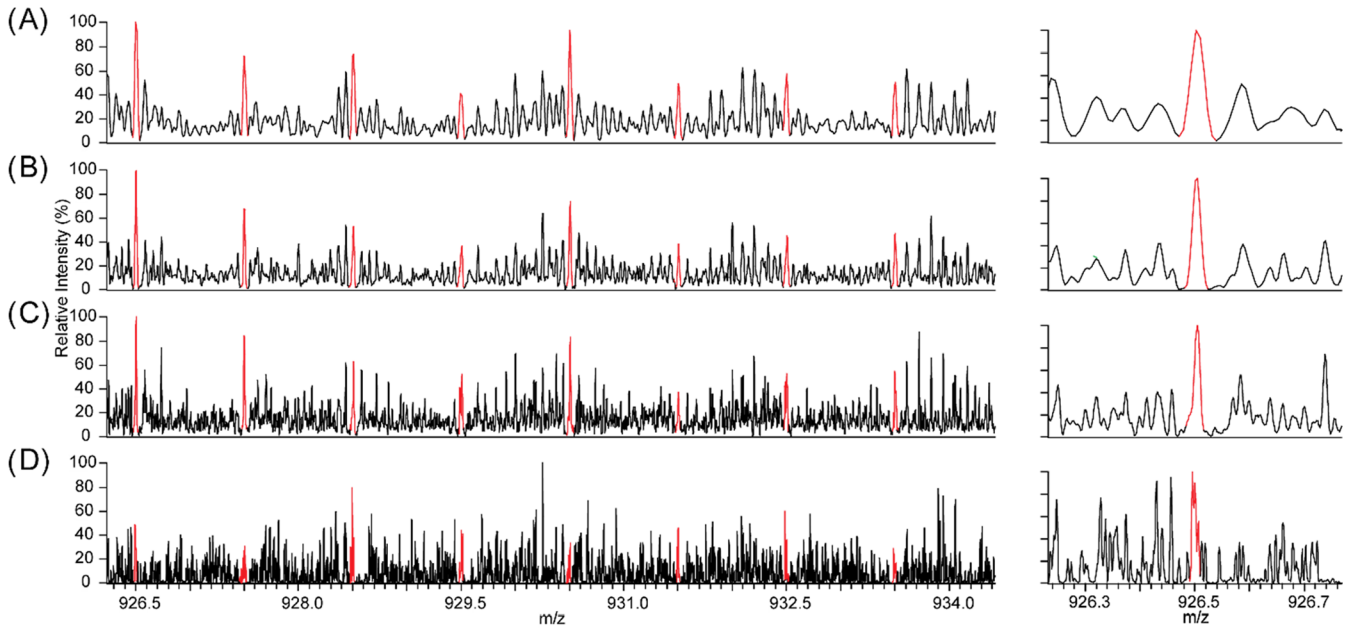


Figure 7. ETD MS^2 spectra of the 21^+ charge state of apomyoglobin acquired at resolving powers of (A) 60,000, (B) 120,000, (C) 240,000, and (D) 500,000 (defined at m/z 200). The left panels show a representative spectral region in which peak intensities decrease with increasing resolving power. The right panels show expanded views of the same spectra centered at m/z 926.5.

not display a picket-fence pattern. Thus, although isotopic distributions introduce small deviations from the simplified model, these deviations are sufficiently small such that the overall reinforcement behavior remains governed by the mass-defect scaling behavior of the underlying sequence. A more detailed discussion of the isotopic considerations is provided in the Supporting Information.

In recent years, there has been increased discussion regarding the utility of assigning internal fragments in intact protein MS/MS spectra.[39,40] We propose that the primary manifestation of internal fragments from dissociation methods that do not exhibit preferential cleavage adjacent to specific amino acid residues (e.g., ETD, ECD, UVPD, EDD, etc.) is the observation of picket fence peak series. For such "democratic" dissociation methods, the yield of any individual internal fragment ion species is significantly lower compared to that of first-generation (single-cleavage events) sequence fragment ion species; however, the total number of unique internal product ion species is vastly greater. For example, consider dissociation of apomyoglobin (153 amino acid residues) in which only a single type of backbone bond cleavage type (e.g., $N-C_\alpha$) is allowed. There are 304 possible unique terminal-containing sequence fragments (e.g., *c*- and *z*•-type ions), whereas over 11,000 internal fragments are possible. Only at the picket fence m/z values does the superposition of signal from multiple internal fragment species reach a scale comparable to that of first-generation fragment ion species. In sufficiently complex spectral regions, this behavior can result in the picket-fence peaks becoming the dominant feature (Figure 1, inset) or, alternatively, distorting isotopic envelopes of terminal fragment ion species (Figure S7).

Resolving Power, Transient Dynamics, and Peak Reinforcement

With this baseline established, we next considered how increased resolving power alters the appearance of reinforced peak patterns without changing their underlying geometric origin. ETD MS^2 spectra of the 20^+ charge state of apomyoglobin were acquired over a range of Orbitrap resolving-power settings (Figure 7). At a nominal resolving power setting of 240,000 (defined at m/z 200), the picket-fence pattern remains readily apparent, indicating that this level of resolving power is insufficient to separate the overlapping fragment-ion signals. Increasing the acquisition time to achieve a resolving power of 500,000 results in a marked reduction in the apparent intensity of the picket-fence m/z peaks and introduces isotopic fine structure at the tops of individual peaks, consistent with partial resolution of the underlying fragment-ion species. Even at this elevated resolving power, however, the contributing fragment ions remain sufficiently close in exact m/z that they cannot be fully resolved under practical experimental conditions. These results indicate that, while very high resolving power can attenuate the picket-fence pattern in favorable cases, resolution alone is insufficient to eliminate the effect in highly congested regions of intact-protein MS/MS spectra.

In addition to partial spectral separation, reductions in the apparent intensity of picket-fence peaks at higher resolving power can arise from signal-processing effects intrinsic to Fourier-transform mass spectrometry. In particular, the interplay between signal decay, the duration of the recorded transient, and apodization influences how fragment-ion signals are weighted over the course of the transient. Prior to Fourier transformation, the digitized ion signal (free induction decay, or FID transient) is typically apodized with symmetric window functions to suppress frequency-domain sidelobe artifacts, resulting in reduced weighting of signal contributions at the beginning and end of the transient. As resolving power is increased by extending the recorded transient duration, early portions of the detected signal lie progressively farther from the center of the window function and are therefore more strongly attenuated.

This behavior reflects general signal-processing characteristics of Fourier-transform mass spectrometry and can be observed across different instrument platforms, ion polarities, and activation methods. As a representative example, Figure S8 shows EDD MS/MS data acquired on a 9.4 T FT-ICR

Downloaded from pubs.acs.org/jamsse/article-pdf/doi/10.1021/jasms.6c00257/6900741/jasms.6c00257.pdf by FLORIDA STATE UNIV user on 02 November 2026

https://doi.org/10.1021/jasms.6c00257
J. Am. Soc. Mass Spectrom. XXXX, XXX, XXX−XXX

instrument, illustrating that the apparent intensity of picket-fence peaks depends strongly on how early transient data are weighted, with weakly apodizing or asymmetric window functions producing more pronounced peak series. Time–frequency analysis provides a more direct and mechanistically revealing view of this effect. Figure S9 shows FT spectra at near-identical resolution generated from successive subsections of the same transient, analyzed without apodization. Early portions of the transient produce pronounced picket-fence patterns, whereas later portions produce a much more muted effect. These observations indicate that the appearance of picket-fence peaks reflects differences in how the signals from fragment-ion populations are weighted over the course of the transient, while the underlying alignment and spacing of contributing m/z values remain unchanged. The stronger contribution of picket-fence peaks in the early portions of the transient is also consistent with their origin from large, highly charged fragment-ion populations. Such ions would generally be expected to exhibit larger collisional cross sections and therefore more rapid transient signal decay than smaller fragment ions of similar m/z, causing them to contribute a disproportionately lower amount to the latter portions of the detected signal. Consequently, the apparent intensity of the picket-fence pattern becomes particularly sensitive to transient length and apodization, which alter the relative weighting of early and late transient contributions.

Taken together, these results demonstrate that increased resolving power can reduce the *apparent* intensity of picket-fence interference peaks through a combination of true spectral resolution and mass-dependent transient signal weighting. In cases where fragment-ion m/z values are strongly aligned and spectral congestion is severe, however, resolution-based approaches alone are insufficient to eliminate the picket-fence pattern.

CONCLUSIONS

Mass-defect-driven signal reinforcement represents an often underappreciated but fundamental challenge in the tandem mass spectrometric analysis of intact biomolecules. As demonstrated here, the superposition of fragment-ion m/z series can give rise to reinforced peak patterns whose spacing and apparent structure resemble those expected for low-charge-state isotopic envelopes, complicating fragment-ion assignment during spectral interpretation. Importantly, the relative scarcity of prior reports of such picket-fence peak series likely reflects historical limitations in data quality and accessible mass range rather than the absence of the phenomenon itself. Related spectral features have been reported previously. For example, Horn, Ge, and McLafferty described a "variable background of small peaks at unit m/z spacing" in activated-ion ECD spectra of ubiquitin, although the origins of these peaks were not established at the time.[41] The present results suggest that similar features can arise through mass-defect-driven reinforcement of highly congested fragment-ion populations.

As advances in instrumentation, sample preparation, and fragmentation methods continue to push intact-protein MS/MS toward higher molecular weights, these reinforcement effects are expected to be encountered more frequently. Similar considerations naturally extend to the mass-spectrometric analysis of oligonucleotides, where a smaller and more uniform set of chemical building blocks leads to more constrained mass-defect behavior, increasing the likelihood of strong m/z reinforcement.

While extremely high resolving power can mitigate some instances of signal reinforcement by partially separating contributing peaks, increased resolution alone is not a general solution. Such experiments typically require specialized and costly instrumentation and may impose significant trade-offs in acquisition speed, sensitivity, and throughput. Moreover, the most severe reinforcement patterns arising from strong mass-defect proportionality across large fragment populations are unlikely to be eliminated solely through increased resolving power.

These results highlight the need for alternative strategies that address the structural origins of mass-defect-driven reinforcement. Charge-state manipulation approaches, such as PTCR alone[9,42] and in combination with PIP,[19,43] redistribute fragment-ion populations in m/z space and have previously been shown to reduce spectral congestion, thereby lessening ambiguity in fragment-ion charge-state assignment and isotopic envelope interpretation in MS/MS spectra. Such charge-reduction approaches would also be expected to disrupt the alignment conditions responsible for the formation of reinforced m/z peak series and associated distortions of isotopic peak-abundance profiles.

Charge-detection mass spectrometry (CDMS) represents another potential strategy for addressing ambiguities associated with highly congested fragment-ion populations because individual ions are measured separately rather than as ensemble signals.[44] Although this approach may reduce some forms of spectral overlap, highly congested fragment-ion populations containing large numbers of species with similar mass-to-charge ratios and charge states may still present challenges. By contrast, PTCR directly redistributes fragment-ion populations in m/z space, reducing overlap among isotopic peak envelopes and facilitating interpretation of dense top-down MS/MS spectra.[9,42]

Equally critical is the development of spectral-interpretation algorithms that explicitly account for mass-defect-driven reinforcement so that reinforced peaks are not misinterpreted as independent isotopic features. Incorporating sequence-specific mass-defect scaling and residual behavior into data-analysis workflows will be essential for robust fragment assignment as top-down proteomics and nucleic-acid mass spectrometry continue to expand toward larger and more complex analytes.

More broadly, this work reframes reinforced peak patterns as a predictable consequence of mass-defect proportionality in highly charged fragment populations, rather than as anomalous or instrument-specific artifacts. By establishing this behavior as a general and intrinsic feature of intact-biomolecule fragmentation, these findings provide a conceptual foundation for interpreting spectral congestion and anticipating the conditions under which reinforcement will arise and influence fragment-ion assignment. Recognizing this behavior therefore shifts reinforced peaks from a source of ambiguity to a diagnostically meaningful indicator of mass-defect proportionality and fragment-ion population structure in complex MS/MS spectra.

ASSOCIATED CONTENT

Supporting Information

The Supporting Information is available free of charge at https://pubs.acs.org/doi/10.1021/jasms.6c00257.

Mass-defect analyses, PTCR experiments, carbonic anhydrase II spectra, isotopic-envelope distortion exam-

Downloaded from pubs.acs.org/jamsef/article-pdf/doi/10.1021/jasms.6c00257/6900474l/jasms.6c00257.pdf by FLORIDA STATE UNIV user on 02 November 2026

https://doi.org/10.1021/jasms.6c00257
J. Am. Soc. Mass Spectrom. XXXX, XXX, XXX−XXX

ples, apodization and time-frequency analyses, simulated isotopic fine structure, supplemental discussion of isotopic considerations, and data availability information (Figures S1−S9) (PDF)

AUTHOR INFORMATION

Corresponding Author

Lissa C. Anderson − *Ion Cyclotron Resonance Program, National High Magnetic Field Laboratory, Tallahassee, Florida 32310, United States; Department of Chemistry and Biochemistry, Florida State University, Tallahassee, Florida 32306, United States;* orcid.org/0000-0001-8633-0251; Email: anderson@magnet.fsu.edu

Authors

Joshua D. Hinkle − *Department of Chemistry, University of Virginia, Charlottesville, Virginia 22904, United States; Thermo Fisher Scientific, San Jose, California 95134, United States*

Steven A. DeFiglia − *Ion Cyclotron Resonance Program, National High Magnetic Field Laboratory, Tallahassee, Florida 32310, United States; Department of Chemistry and Biochemistry, Florida State University, Tallahassee, Florida 32306, United States*

Robert A. D'Ippolito − *Department of Chemistry, University of Virginia, Charlottesville, Virginia 22904, United States*

Christopher Mullen − *Thermo Fisher Scientific, San Jose, California 95134, United States*

Greg T. Blakney − *Ion Cyclotron Resonance Program, National High Magnetic Field Laboratory, Tallahassee, Florida 32310, United States;* orcid.org/0000-0002-4205-9866

Ping Yip − *Thermo Fisher Scientific, San Jose, California 95134, United States*

Romain Huguet − *Thermo Fisher Scientific, San Jose, California 95134, United States*

Kristina Håkansson − *Ion Cyclotron Resonance Program, National High Magnetic Field Laboratory, Tallahassee, Florida 32310, United States; Department of Chemistry and Biochemistry, Florida State University, Tallahassee, Florida 32306, United States;* orcid.org/0000-0003-1926-0542

Jeffrey Shabanowitz − *Department of Chemistry, University of Virginia, Charlottesville, Virginia 22904, United States;* orcid.org/0000-0001-5750-3539

Donald F. Hunt − *Department of Chemistry, University of Virginia, Charlottesville, Virginia 22904, United States*

John E. P. Syka − *Thermo Fisher Scientific, San Jose, California 95134, United States*

Complete contact information is available at: https://pubs.acs.org/10.1021/jasms.6c00257

Notes

The authors declare the following competing financial interest(s): Joshua D. Hinkle and Christopher Mullen are current employees of the Life Sciences Mass Spectrometry (LSMS) business of Thermo Fisher Scientific Co., and Ping Yip and John E. P. Syka are former employees of LSMS. Thermo Fisher Scientific manufactures the Orbitrap Eclipse, Fusion, Fusion Lumos, and Orbitrap Elite instruments used in this work.

ACKNOWLEDGMENTS

The authors gratefully acknowledge Nathan K. Kaiser, Chad R. Weisbrod, Sean D. Dunham, Christopher L. Hendrickson, and the Pitteri laboratory (Stanford University) for instrumental assistance and valuable discussions. S.A.D. was supported by NSF grant CHE-2528759 to K.H. J.D.H., R.A.D., and J.S. were supported by NIH grant GM037357 to D.F.H. A portion of this work was performed at the Ion Cyclotron Resonance Facility at the National High Magnetic Field Laboratory at Florida State University, supported by the National Science Foundation Divisions of Materials Research and Chemistry (DMR-1644779 and DMR-2128556) and by the State of Florida. The authors respectfully acknowledge the profound and lasting contributions of Professor Alan G. Marshall to the field of Fourier transform mass spectrometry. His pioneering work in FT-ICR and his leadership in establishing the Ion Cyclotron Resonance program at the National High Magnetic Field Laboratory have fundamentally shaped modern mass spectrometry. The concepts and measurements described in this work are made possible in part by this legacy, which continues to influence both the instrumentation and interpretation of high-resolution mass spectra. Portions of the writing and figure preparation for this manuscript were assisted by artificial intelligence (AI) tools, and all outputs were reviewed and edited by the authors for accuracy and scientific content. The content is solely the responsibility of the authors and does not necessarily represent the official views of the funding agencies.

REFERENCES

(1) Chi, A.; Bai, D. L.; Geer, L. Y.; Shabanowitz, J.; Hunt, D. F. Analysis of intact proteins on a chromatographic time scale by electron transfer dissociation tandem mass spectrometry. *Int. J. Mass Spectrom.* **2007**, *259*, 197−203.

(2) Toby, T. K.; Fornelli, L.; Kelleher, N. L. Progress in top-down proteomics and the analysis of proteoforms. *Annu. Rev. Anal. Chem.* **2016**, *9*, 499−519.

(3) Gault, J.; Malosse, C.; Machata, S.; Millien, C.; Podglajen, I.; Ploy, M. C.; Costello, C. E.; Duménil, G.; Chamot-Rooke, J. Complete posttranslational modification mapping of pathogenic Neisseria meningitidis pilins requires top-down mass spectrometry. *Proteomics* **2014**, *14* (10), 1141−1151.

(4) Coelho Graça, D.; Hartmer, R.; Jabs, W.; Beris, P.; Clerici, L.; Stoermer, C.; Samii, K.; Hochstrasser, D.; Tsybin, Y. O.; Scherl, A.; Lescuyer, P. Identification of hemoglobin variants by top-down mass spectrometry using selected diagnostic product ions. *Anal. Bioanal. Chem.* **2015**, *407* (10), 2837−2845.

(5) Tran, J. C.; Zamdborg, L.; Ahlf, D. R.; Lee, J. E.; Catherman, A. D.; Durbin, K. R.; Tipton, J. D.; Vellaichamy, A.; Kellie, J. F.; Li, M.; Wu, C.; Sweet, S. M. M.; Early, B. P.; Siuti, N.; LeDuc, R. D.; Compton, P. D.; Thomas, P. M.; Kelleher, N. L. Mapping intact protein isoforms in discovery mode using top-down proteomics. *Nature* **2011**, *480* (7376), 254.

(6) Anderson, L. C.; Karch, K. R.; Ugrin, S. A.; Coradin, M.; English, A. M.; Sidoli, S.; Shabanowitz, J.; Garcia, B. A.; Hunt, D. F. Analyses of histone proteoforms using front-end electron transfer dissociation-enabled Orbitrap instruments. *Mol. Cell Proteomics* **2016**, *15* (3), 975−988.

(7) Krokhin, O. V.; Antonovici, M.; Ens, W.; Wilkins, J. A.; Standing, K. G. Deamidation of -Asn-Gly- Sequences during Sample Preparation for Proteomics: Consequences for MALDI and HPLC-MALDI Analysis. *Anal. Chem.* **2006**, *78* (18), 6645−6650.

(8) Dang, X.; Scotcher, J.; Wu, S.; Chu, R. K.; Tolić, N.; Ntai, I.; Thomas, P. M.; Fellers, R. T.; Early, B. P.; Zheng, Y.; Durbin, K. R.; LeDuc, R. D.; Wolff, J. D.; Thompson, C. J.; Pan, J.; Han, J.; Shaw, J. B.; Salisbury, J. P.; Easterling, M.; Borchers, C. H.; Brodbelt, J. S.; Agar, J. N.; Paša-Tolić, L.; Kelleher, N. L.; Young, N. L. The first pilot project of the consortium for top-down proteomics: A status report. *Proteomics* **2014**, *14* (10), 1130−1140.

Downloaded from pubs.acs.org/jamsef/article-pdf/doi/10.1021/jasms.6c00257/6900741/jasms.6c00257.pdf by FLORIDA STATE UNIV user on 02 November 2026

(9) Anderson, L. C.; English, A. M.; Wang, W. H.; Bai, D. L.; Shabanowitz, J.; Hunt, D. F. Protein derivatization and sequential ion/ion reactions to enhance sequence coverage produced by electron transfer dissociation mass spectrometry. *Int. J. Mass Spectrom.* **2015**, *377*, 617−624.
(10) Riley, N. M.; Westphall, M. S.; Coon, J. J. Activated Ion-Electron Transfer Dissociation Enables Comprehensive Top-Down Protein Fragmentation. *J. Proteome Res.* **2017**, *16* (7), 2653−2659.
(11) Fornelli, L.; Toby, T. K. Characterization of large intact protein ions by mass spectrometry: What directions should we follow? *Biochim. Biophys. Acta, Proteins Proteomics* **2022**, *1870* (4), No. 140758.
(12) Mann, M. Useful tables of possible and probable peptide masses. In *Proceedings of the 43rd ASMS Conference on Mass Spectrometry and Allied Topics*, Atlanta, GA, May, 1995.
(13) Mitra, I.; Nefedov, A. V.; Brasier, A. R.; Sadygov, R. G. Improved Mass Defect Model for Theoretical Tryptic Peptides. *Anal. Chem.* **2012**, *84* (6), 3026−3032.
(14) Srzentic, K.; Fornelli, L.; Tsybin, Y. O.; Loo, J. A.; Seckler, H.; Agar, J. N.; Anderson, L. C.; Bai, D. L.; Beck, A.; Brodbelt, J. S.; van der Burgt, Y. E. M.; Chamot-Rooke, J.; Chatterjee, S.; Chen, Y.; Clarke, D. J.; Danis, P. O.; Diedrich, J. K.; D'Ippolito, R. A.; Dupre, M.; Gasilova, N.; Ge, Y.; Goo, Y. A.; Goodlett, D. R.; Greer, S.; Haselmann, K. F.; He, L.; Hendrickson, C. L.; Hinkle, J. D.; Holt, M. V.; Hughes, S.; Hunt, D. F.; Kelleher, N. L.; Kozhinov, A. N.; Lin, Z.; Malosse, C.; Marshall, A. G.; Menin, L.; Millikin, R. J.; Nagornov, K. O.; Nicolardi, S.; Paša-Tolić, L.; Pengelley, S.; Quebbemann, N. R.; Resemann, A.; Sandoval, W.; Sarin, R.; Schmitt, N. D.; Shabanowitz, J.; Shaw, J. B.; Shortreed, M. R.; Smith, L. M.; Sobott, F.; Suckau, D.; Toby, T.; Weisbrod, C. R.; Wildburger, N. C.; Yates III, J. R.; Yoon, S. H.; Young, N. L.; Zhou, M. Interlaboratory study for characterizing monoclonal antibodies by top-down and middle-down mass spectrometry. *J. Am. Soc. Mass Spectrom.* **2020**, *31* (9), 1783−1802.
(15) Earley, L.; Anderson, L. C.; Bai, D. L.; Mullen, C.; Syka, J. E. P.; English, A. M.; Dunyach, J.; Stafford, G. C., Jr; Shabanowitz, J.; Hunt, D. F.; Compton, P. D. Front-end electron transfer dissociation: a new ionization source. *Anal. Chem.* **2013**, *85* (17), 8385−8390.
(16) Coon, J. J.; Ueberheide, B.; Syka, J. E. P.; Dryhurst, D. D.; Ausio, J.; Shabanowitz; Hunt, D. F. Protein identification using sequential ion/ion reactions and tandem mass spectrometry. *Proc. Natl. Acad. Sci. U.S.A.* **2005**, *102*, 9463−9468.
(17) McLuckey, S. A.; Reid, G. E.; Wells, J. M. Ion parking during ion/ion reactions in electrodynamic ion traps. *Anal. Chem.* **2002**, *74*, 336−346.
(18) Reid, G. E.; Shang, H.; Hogan, J. M.; Lee, G. U.; McLuckey, S. A. Gas-phase concentration, purification, and identification of whole proteins from complex mixtures. *J. Am. Chem. Soc.* **2002**, *124*, 7353−7362.
(19) Ugrin, S. A.; English, A. M.; Syka, J. E.; Bai, D. L.; Anderson, L. C.; Shabanowitz, J.; Hunt, D. F. Ion-ion proton transfer and parallel ion parking for the analysis of mixtures of intact proteins on a modified Orbitrap mass analyzer. *J. Am. Soc. Mass Spectrom.* **2019**, *30* (10), 2163−2173.
(20) Stephenson, J. L.; McLuckey, S. A. Ion/Ion proton transfer reactions for protein mixture analysis. *Anal. Chem.* **1996**, *68*, 4026−4032.
(21) Chrisman, P. A.; Pitteri, S. J.; McLuckey, S. A. Parallel Ion Parking: Improving Conversion of Parents to First Generation Products in Electron Transfer Dissociation. *Anal. Chem.* **2005**, *77*, 3411−3414.
(22) Lutomski, C. A.; El-Baba, T. J.; Hinkle, J. D.; Liko, I.; Bennett, J. L.; Kalmankar, N. V.; Dolan, A.; Kirschbaum, C.; Greis, K.; Urner, L. H.; Kapoor, P.; Yen, H. Y.; Pagel, K.; Mullen, C.; Syka, J. E. P.; Robinson, C. V. Infrared Multiphoton Dissociation Enables Top-Down Characterization of Membrane Protein Complexes and G Protein-Coupled Receptors. *Angew. Chem., Int. Ed.* **2023**, *62* (36), No. e202305694.
(23) Ganisl, B.; Taucher, M.; Riml, C.; Breuker, K. Charge as you like! Efficient manipulation of negative ion net charge in electrospray ionization of proteins and nucleic acids. *Eur. J. Mass Spectrom.* **2011**, *17*, 333−343.
(24) Senko, M. W.; Hendrickson, C. L.; Paša-Tolić, L.; Marto, J. A.; White, F. M.; Guan, S.; Marshall, A. G. Electrospray Ionization Fourier Transform Ion Cyclotron Resonance at 9.4 T. *Rapid Commun. Mass Spectrom.* **1996**, *10*, 1824−1828.
(25) Kaiser, N. K.; Quinn, J. P.; Blakney, G. T.; Hendrickson, C. L.; Marshall, A. G. A novel 9.4 Tesla FTICR mass spectrometer with improved sensitivity, mass resolution, and mass range. *J. Am. Soc. Mass Spectrom.* **2011**, *22*, 1343−1351.
(26) Tolmachev, A. V.; Robinson, E. W.; Smith, R. D.; Leach, F. E.; Futrell, J. H.; Paša-Tolić, L. A Conceptual Approach for FT-ICR Cell Harmonization Utilizing External Shim Electrodes. *Int. J. Mass Spectrom.* **2012**, *325*−*327*, 45−50.
(27) Kaiser, N. K.; Savory, J. J.; McKenna, A. M.; Quinn, J. P.; Hendrickson, C. L.; Marshall, A. G. Electrically Compensated Fourier Transform Ion Cyclotron Resonance Cell for Complex Mixture Mass Analysis. *Anal. Chem.* **2011**, *83* (17), 6907−6910.
(28) Budnik, B. A.; Haselmann, K. F.; Zubarev, R. A. Electron Detachment Dissociation of Peptide Di-Anions: An Electron−Hole Recombination Phenomenon. *Chem. Phys. Lett.* **2001**, *342* (3), 299−302.
(29) Ganisl, B.; Valovka, T.; Hartl, M.; Taucher, M.; Bister, K.; Breuker, K. Electron Detachment Dissociation for Top-Down Mass Spectrometry of Acidic Proteins. *Chem.—Eur. J.* **2011**, *17* (16), 4460−4469.
(30) Song, H.; Håkansson, K. Electron Detachment Dissociation and Negative Ion Infrared Multiphoton Dissociation of Electrosprayed Intact Proteins. *Anal. Chem.* **2012**, *84* (2), 871−876.
(31) Yang, J.; Håkansson, K. Characterization and optimization of electron detachment dissociation Fourier transform ion cyclotron resonance mass spectrometry. *Int. J. Mass Spectrom.* **2008**, *276*, 144−148.
(32) Blakney, G. T.; Hendrickson, C. L.; Marshall, A. G. Predator data station: A fast data acquisition system for advanced FT-ICR MS experiments. *Int. J. Mass Spectrom.* **2011**, *306*, 246−252.
(33) Sejdić, E.; Djurović, I.; Jiang, J. Time−Frequency Feature Representation Using Energy Concentration: An Overview of Recent Advances. *Digital Signal Process.* **2009**, *19*, 153−183.
(34) Wang, M.; Huang, W. J.; Kondev, F. G.; Audi, G.; Naimi, S. The AME 2020 atomic mass evaluation (II). Tables, graphs and references*. *Chin. Phys. C* **2021**, *45* (3), No. 030003.
(35) Takeuchi, T.; McQuillan, A. J.; Shard, A.; Russell, A. E.; Hibbert, D. B. Glossary of methods and terms used in surface chemical analysis (IUPAC Recommendations 2020). *Pure Appl. Chem.* **2020**, *92* (11), 1781−1860.
(36) Yergey, J.; Heller, D.; Hansen, G.; Cotter, R. J.; Fenselau, C. Isotopic Distributions in Mass Spectra of Large Molecules. *Anal. Chem.* **1983**, *55*, 353−356.
(37) Sleno, L. The use of mass defect in modern mass spectrometry. *J. Mass. Spectrom.* **2012**, *47*, 226−236.
(38) Senko, M. W.; Beu, S. C.; McLafferty, F. W. Determination of Monoisotopic Masses and Ion Populations for Large Biomolecules from Resolved Isotopic Distributions. *J. Am. Soc. Mass Spectrom.* **1995**, *6* (4), 229−233.
(39) Mikawy, N. N.; Rojas Ramírez, C.; DeFiglia, S. A.; Szot, C. W.; Le, J.; Lantz, C.; Wei, B.; Zenaidee, M. A.; Blakney, G. T.; Nesvizhskii, A. I.; Loo, J. A.; Ruotolo, B. T.; Shabanowitz, J.; Anderson, L. C.; Håkansson, K. Are Internal Fragments Observable in Electron Based Top-Down Mass Spectrometry? *Mol. Cell. Proteomics* **2024**, *23*, No. 100814.
(40) Derbez-Morin, M.; Julian, R. R. Statistical Considerations for the Assignment of Internal Ions in Top-Down Mass Spectrometry. *Anal. Sens.* **2026**, *6* (2), No. e202500153.
(41) Horn, D. M.; Ge, Y.; McLafferty, F. W. Activated Ion Electron Capture Dissociation for Mass Spectral Sequencing of Larger (42 kDa) Proteins. *Anal. Chem.* **2000**, *72* (20), 4778−4784.
(42) Huguet, R.; Mullen, C.; Srzentić, K.; Greer, J. B.; Fellers, R. T.; Zabrouskov, V.; Syka, J. E. P.; Kelleher, N. L.; Fornelli, L. Proton

Downloaded from pubs.acs.org/jamsef/article-pdf/doi/10.1021/jasms.6c00257/6900741/jasms.6c00257.pdf by FLORIDA STATE UNIV user on 02 November 2026

Transfer Charge Reduction Enables High-Throughput Top-Down Analysis of Large Proteoforms. *Anal. Chem.* **2019**, *91*, 15732−15739.
(43) Weisbrod, C. R.; Anderson, L. C.; Hendrickson, C. L.; Schaffer, L. V.; Shortreed, M. R.; Smith, L. M.; Shabanowitz, J.; Hunt, D. F. Advanced Strategies for Proton-Transfer Reactions Coupled with Parallel Ion Parking on a 21 T FT-ICR MS for Intact Protein Analysis. *Anal. Chem.* **2021**, *93* (26), 9119−9128.
(44) Kafader, J. O.; Durbin, K. R.; Melani, R. D.; Des Soye, B. J.; Schachner, L. F.; Senko, M. W.; Compton, P. D.; Kelleher, N. L. Individual Ion Mass Spectrometry Enhances the Sensitivity and Sequence Coverage of Top-Down Mass Spectrometry. *J. Proteome Res.* **2020**, *19* (3), 1346−1350.

Downloaded from pubs.acs.org/jamsef/article-pdf/doi/10.1021/jasms.6c00257/6900474l/jasms.6c00257.pdf by FLORIDA STATE UNIV user on 02 November 2026

https://doi.org/10.1021/jasms.6c00257
J. Am. Soc. Mass Spectrom. XXXX, XXX, XXX−XXX